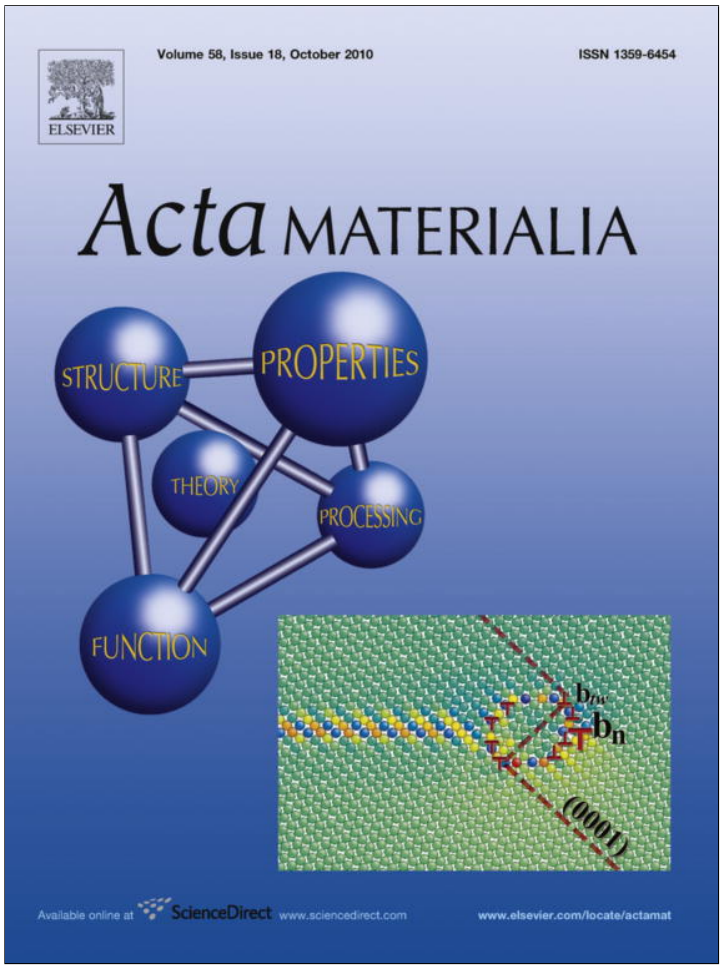

Available online at www.sciencedirect.com
ScienceDirect
Acta Materialia 58 (2010) 6055–6063
Acta MATERIALIA
www.elsevier.com/locate/actamat

Mechanical and microstructural single-crystal Bauschinger effects: Observation of reversible plasticity in copper during bending

Eralp Demir, Dierk Raabe *

Max-Planck-Institut für Eisenforschung, Max-Planck Str. 1, 40237 Düsseldorf, Germany

Received 25 May 2010; received in revised form 10 July 2010; accepted 11 July 2010
Available online 25 August 2010

Abstract

We study the Bauschinger effect on a bent and straightened micro-sized single-crystal copper beam (width: 8.64 μm; thickness: 7.05 μm) over three consecutive cycles. The reverse yield strengths (straightening step) are much smaller than those in forward loading (bending step). An upper bound estimate shows a load drop of 73% (1st cycle), 76% (2nd cycle) and 83% (3rd cycle) relative to the forward yield stress. Electron backscatter diffraction reveals a dramatic reduction in the bending-induced misorientation gradients upon load reversal (straightening), documenting an unexpected form of microstructure reversibility. The observed Bauschinger softening is interpreted in terms of two effects. The first consists of internal backstresses that support load reversal. They are created by polarized dislocation arrays that are accumulated during forward bending. The second effect is the reduced requirement to activate dislocation sources during reverse loading as the dislocations that were stored during bending did not participate much in cross-hardening and, hence, serve as mobile dislocations upon reverse loading. After straightening the misorientation gradients are largely removed but the non-polarized dislocations remain. We therefore introduce a revised terminology, namely the "mechanical Bauschinger effect" and the "microstructural Bauschinger effect". The former term describes a yield stress drop and the latter one the degree of microstructure reversibility upon load path changes.

Keywords: Bauschinger effect; Plastic deformation; Electron backscattering diffraction (EBSD); Copper

1. Introduction

The Bauschinger effect is characterized by a reduction in yield strength upon load reversal or load path change [1,2]. In polycrystals it is mainly attributed to polarized dislocations (dislocations of the same sign) in front of interfaces [3]. In single crystals it is interpreted in terms of cell wall structures that are polarized through accumulated dislocations during forward loading [4,5]. In either case long-range backstresses gradually build up that resist further forward loading but reduce the yield strength when reversing the sense of the applied load [1,6]. In addition to the backstress effect induced by dislocation polarization it was suggested that the removal of dislocation loops and untangling of dislocations from obstacles (i.e. cell walls) upon load reversal releases mobile dislocations [7]. Thus enhanced availability of mobile dislocations reduces the requirement to activate new dislocation sources. This leads to softer reverse response and a smooth transition between the elastic and elastic–plastic regimes in the reverse stress–strain curves.

The Bauschinger effect has important consequences for any inelastic deformation where materials are exposed to strain path and loading changes. At the macroscopic scale such boundary conditions apply to practically all operations in metal forming. At the microscopic scale many components such as microelectromechanical devices (MEMS) or metallic compounds in thermally loaded electronic parts are exposed to such cyclic forward and backward straining [14]. While some investigations have addressed the Bauschinger effect at the macroscopic and polycrystal scale [1,2,8,9], only a few corresponding studies have been

* Corresponding author. Tel.: +49 211 6792 278.
E-mail address: d.raabe@mpie.de (D. Raabe).

1359-6454/$36.00 © 2010 Acta Materialia Inc. Published by Elsevier Ltd. All rights reserved.
doi:10.1016/j.actamat.2010.07.023

published on micrometer-sized single-crystal testing and simulation [10–14]. For this reason we investigate in this work the origin of the Bauschinger effect in an experimental approach by using a microscale single-crystal cantilever beam exposed to a sequence of bending–straightening cycles in an indenter device (Fig. 1).

2. Experimental

A single-crystal copper sample was grown in a Bridgman furnace. A cylindrical specimen with a diameter of 100 μm was manufactured by wire electrodischarge grinding followed by etching in a 40% HNO_3 solution. From this specimen a cantilever beam was cut by focused ion beam (FIB) milling using 500 pA at 30 keV as finishing current for all surfaces. The final width and thickness of the beam were 8.64 μm and 7.05 μm, respectively (Fig. 1). The beam was exposed to three deformation cycles (bending and straightening) comprising six individual loading tests. The beam had initial Bunge–Euler angles of $\varphi_1 = 260.0$, $\phi = 101.1$, $\varphi_2 = 248.2$ (Fig. 1). The corresponding Miller indices are [−5 2 1] for the longitudinal beam axis, [4 −1 1 2] for the transverse direction and [5 2 21] for the loading axis (indicated by $+x$ in Fig. 1). After ex situ electron backscatter diffraction (EBSD) characterization of the starting microstructure in a scanning electron microscope the sample was mounted in a Hysitron indenter device for loading. The cantilever beam was bent with a displacement of 3 μm at a rate of 1 μm s^{-1} in displacement-controlled mode. Subsequent ex situ microstructural characterization of the texture was performed using EBSD. For straightening, the same ex situ procedure consisting of deformation in an indenter and subsequent characterization in an EBSD was applied at the same strain rate.

The motivation for imposing a bending load was that it necessarily leads to the evolution of polarized dislocation structures, namely geometrically necessary dislocations (GNDs), to accommodate the lattice curvature [15–22]. The rationale behind that was to enhance GND-related microstructure polarization and, hence, the Bauschinger effect [1–5]. The assumption that the yield strength asymmetry upon load reversal is essentially due to backstresses (induced by dislocation polarization) and to the remobilization of dislocations from obstacles (i.e. cell walls) suggests that GNDs would make this effect more visible than non-polarized arrays consisting of statistically stored dislocations.

We designed a beam with micrometer dimensions as the accumulation of GNDs in a bent sample is size dependent [16,23,24,15,25,26]. As stated above, it is likely that the resulting backstress will also be enhanced as the size of the specimen is reduced. On the other hand, in order to reduce shear localizations [27,28] and the influence of ion beam damage, we chose a beam thickness above 5 μm.

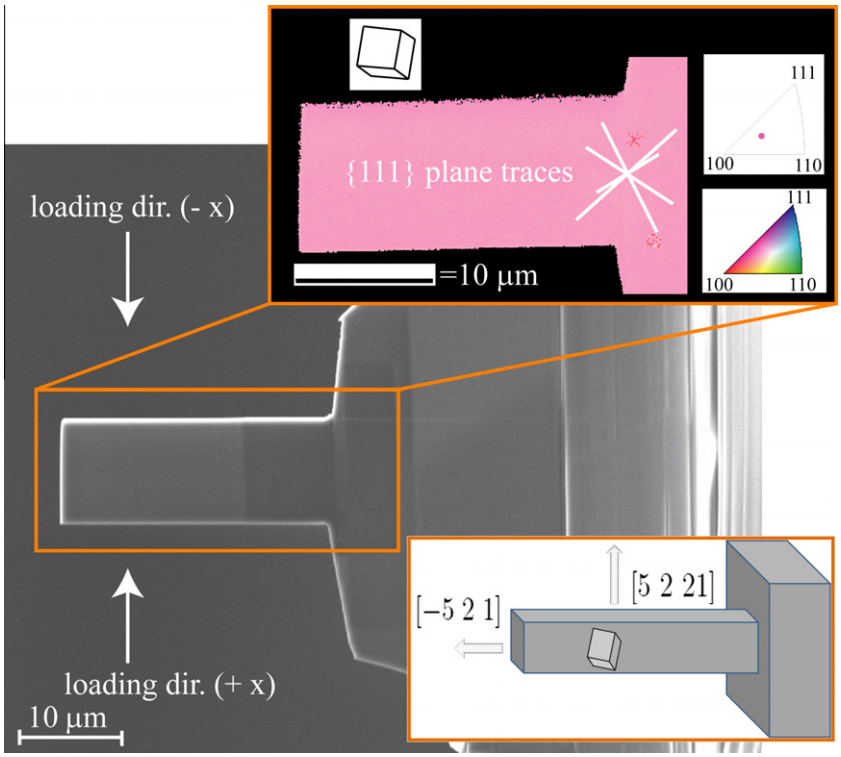

Fig. 1. Longitudinal side view of the copper single-crystal cantilever beam after FIB milling before bending. $+x$ indicates the bending direction and $-x$ the subsequent straightening direction, respectively. The single crystal orientation is given in terms of an EBSD map using inverse pole figure (IPF) color coding.

3. Results

The stress–strain curves shown in Fig. 2 were obtained from force–displacement measurements. For this purpose the bending stress, σ, was used as a measure for the stress using $\sigma = \frac{4F \cdot y}{w \cdot t^2}$ where F,y, w and t are force, moment arm, width and thickness of the beam, respectively [15,16]. The corresponding strain measure, ϵ, was found by normalizing the displacements, d, with the moment arms y, i.e. $\epsilon = 0.3\frac{d}{y}$. The scaling factor 0.3 was estimated from the curvature radius of the bent beams, $1/\kappa$, and used to convert the d/y-ratio into a strain measure (Fig. 2, bottom image). Fig. 2 shows three sets of experiments each comprising an initial bending step followed by a straightening step. The cycles were applied subsequently to the same specimen in a set of experiments consisting of deformation in the indenter and ex situ characterization by EBSD. The curves are plotted on top of each other rather than in classical path-dependent diagrams (using positive and negative axes) for better comparison.

The flow curves show a strong Bauschinger effect in terms of three main phenomena: (i) all three subsequent bending–straightening experiments reveal a strongly reduced yield strength upon load reversal (different possible approaches to quantify an appropriate yield strength measure are discussed below); (ii) all three sets of curves show a very smooth (rounded) transition between the elastic and the elastic–plastic regimes in the straightening steps (Fig. 2); (iii) the microstructure, more specifically, the local misorientation gradient patterns that are formed during bending, are partially removed during subsequent straightening (Fig. 3).

In the following we describe these three key observations in more detail. The first forward bending step (Fig. 2, red solid line) is characterized by yield beginning at a stress of about 170 MPa. The yield values are taken at the intersection of the elastic regime and the back-extrapolated stage I hardening regime. The transition between stage I and stage II hardening is indicated in Fig. 2 by the blue arrows. It should be noted that the transition between

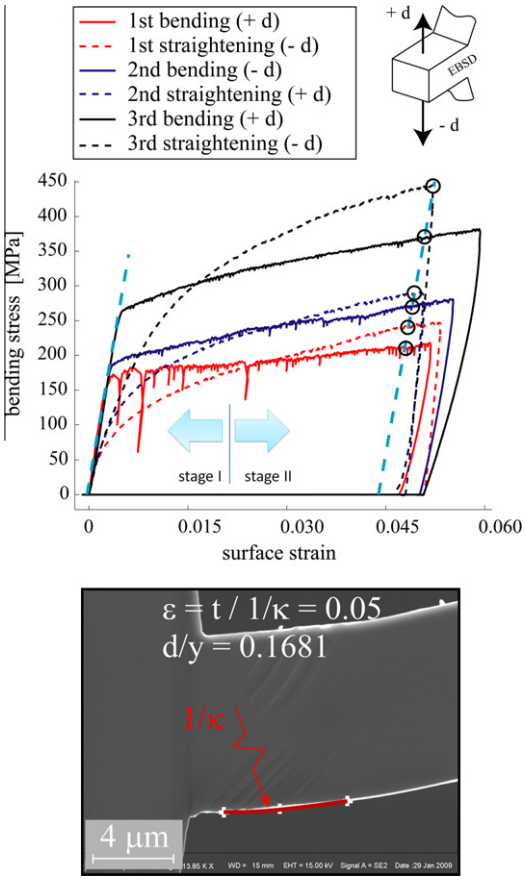

Fig. 2. Stress–strain curves for three subsequent sets of bending–straightening experiments. The first bending (solid line) and straightening (dashed line) curves are in red color. The stress–strain data sets of the following tests are in blue and black, respectively. An approximate scaling of 0.3 is measured from the radius of curvature ($1/\kappa$) of the beams after bending (SEM image, bottom) and used to calculate the strain (ϵ) from the displacement-to-moment arm ratio (d/y). The transition between stage I and stage II hardening was estimated from the derivative of the first bending curve (Fig. 2, red solid line) as indicated by the blue arrows. The stage I/II transition can only be derived from the first bending experiment owing to the increasing influence of isotropic hardening during further cycling. The stages I and II slopes are used for defining upper and lower bound measures for the yield strength.

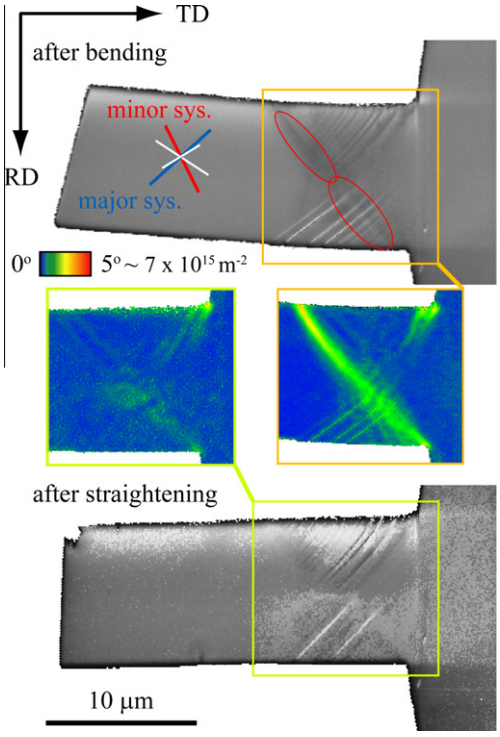

Fig. 3. Kernel average misorientation (KAM, local lattice curvature) and EBSD image-quality maps of the deformed beam after the first bending and straightening test. The KAM measure was obtained by calculating the misorientation gradient of each EBSD data point relative to its first, second and third nearest-neighbor points. The confidence index was higher than 0.1 for all EBSD points. A KAM map (color map) is a measure of the local lattice curvature, and hence of the GND density, and the EBSD image-quality map (grayscale map) is a measure of the statistically stored dislocation density.

stages I and II can only be derived from the first bending experiment owing to the increasing influence of isotropic hardening during further cycling. For the other experiments the linear stage I regime used for the back-extrapolation is also taken to be limited by the position of the two blue arrows.

The first forward bending curve reveals a number of steep stress drops which indicate strong strain bursts. The first and second (large) bursts are characterized by stress drops of more than 60 and 120 MPa, respectively. Upon reverse loading (first straightening step, red dotted curve) plastic yielding already starts at a much smaller stress level, namely at about 45 MPa. The reverse loading curve is very smooth and does not reveal such significant stress drops as the bending curve does. The strain-hardening behavior is more uniform than during initial forward bending. This difference in yield stress between the first bending and the first straightening steps amounts to about 73%. The second bending step (Fig. 2, solid blue line) shows a higher yield stress of about 185 MPa, i.e. it is about 15 MPa above the yield stress observed for the first bending step. Interestingly, the second straightening test (Fig. 2, dotted blue line) starts to yield at about the same stress as the first straightening curve, namely at about 45 MPa. This corresponds to a yield stress difference of about 76% upon load reversal in the second bending–straightening cycle. The third bending step reveals again a higher yield stress of about 265 MPa. Upon load reversal (straightening) inelastic yielding occurs at a very small stress of about 45 MPa, i.e. at about the same value as observed for the two preceding reverse-loading steps. This corresponds to an enormous yield stress difference of about 83% upon load reversal in the third bending–straightening cycle. It must be considered here that possible changes in the exact moment arm and contact conditions imposes an experimental scatter of the stress values of about 5% as discussed in more detail below.

The EBSD map taken after the first bending step reveals the formation of strong misorientation patterning (color maps) (Fig. 3). The local misorientation gradients are here described in terms of the kernel average misorientation (KAM). This is a measure that quantifies the average misorientation gradient around an EBSD point with respect to a defined set of neighbor points (here the first, second and third-nearest neighbor shells were used, each with different weight). As the KAM value captures the magnitude of the local lattice curvature around an EBSD point it serves as an approximate measure of the local GND content [31,32]. The unexpected strong reduction in the KAM patterns after straightening substantiates (incomplete) reversibility of the plastic deformation, more specifically of the GND patterning that was induced during bending (Figs. 3 and 4). Besides the evaluation of the GNDs from the KAM patterns, the grayscale maps, which show the EBSD pattern quality, can be used as a further measure of the local lattice defect density. These image-quality maps reveal areas of residual distortion in the material also after straightening. This means that the local lattice curvature (KAM) is reduced but some of the statistical dislocation content (which is not associated with local rotations) is preserved after reverse loading.

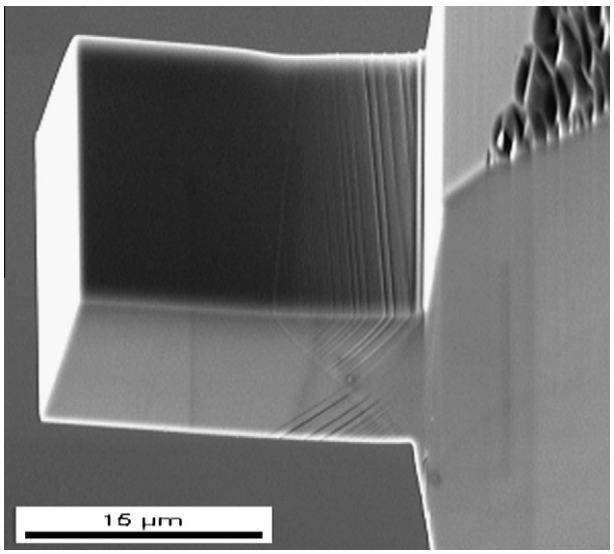

Fig. 4. SEM image revealing the slip traces and slip surface steps created by the two active slip systems.

The accumulation of the localized lattice curvature (KAM patterning) along the slip system traces observed after bending suggest the activity of one major slip system (indicated by the blue line in Fig. 3). In addition, shear localizations along a secondary slip system with minor shear contribution (indicated by the red color in Fig. 3) appear in the EBSD image quality maps, in the KAM (lattice curvature) maps, and also in the SEM slip trace analysis (Fig. 4). The intense misorientation gradient traces around those regions that show high shear localizations (Figs. 3 and 4) indicate a cumulative effect of shear on the minor slip system and the pile-up and polarized debris of dislocations on the major slip system at the border of the shear zone (indicated by red ellipses in Fig. 3).

In addition to these microstructure changes the local stress states must also be considered. The KAM image in Fig. 3 and the slip traces in Fig. 4 suggest the occurrence of stress concentrations and a multiaxial stress state, and, hence, possibly also of multiple slip system activation in association with additional local forest hardening at the corner positions of the cantilever beam (transition zone between bulk and beam). The formation of such distinct slip bands was also observed in discrete dislocation simulations published recently by Kiener et al. [13]. This stress concentration effect underlines the importance of properly monitoring the boundary conditions in small-scale mechanical tests and the requirement to accompany them by discrete dislocation or crystal plasticity finite-element simulations [13,33–35,35–37].

Another macroscopic mechanical effect is the slight variation in the moment arms (y) as quantified in Table 1. The angular rotation of the beam (θ) and the misorientation

Table 1
Direction of beam displacement (dir.), type of deformation (type), moment arm (y, μm), total rotation angle of the beam measured after deformation (θ, deg), the components of the rotation axis along the principal directions, the constants of the linear fit (p_1 and p_2, MPa) to the linear stage II hardening portion of the stress–strain curve.

Dir.	Type	y (μm)	θ (deg)	Av. rot. axis comp.			$f(d) = p_1 d + p_2$	
				RD	TD	ND	p_1 (MPa)	p_2 (MPa)
+d	Bending	17.39	13.69 ± 0.30	0.31 ± 0.02	0.35 ± 0.00	0.88 ± 0.01	824	167.8
−d	Straightening	16.90	0.74 ± 0.23	0.25 ± 0.13	0.56 ± 0.06	0.78 ± 0.08	2476	122.7
−d	Bending	16.32	14.46 ± 0.19	0.22 ± 0.02	0.43 ± 0.00	0.88 ± 0.01	1634	190.8
+d	Straightening	17.78	2.04 ± 0.27	0.06 ± 0.05	0.62 ± 0.05	0.78 ± 0.04	2540	168.3
+d	Bending	15.20	12.35 ± 0.14	0.20 ± 0.03	0.31 ± 0.08	0.93 ± 0.02	2011	269.1
−d	Straightening	17.27	2.02 ± 0.49	0.12 ± 0.13	0.33 ± 0.20	0.91 ± 0.10	3977	251.7

components were measured after each loading step (Table 1). The indenter produced a contact mark on the top surface of the specimen. The size of the indented region (approximately 2 μm^3 for 1 μm contact radius) was much smaller than the bent volume. For 8.64 and 7.05 μm beam dimensions and an average deformed width of 3 μm, the deformed volume was approximately 180 μm^3. Moreover, the indented region (contact point between tool and beam) was far away from the region where the bending was finally localized, i.e. close to the transition region between the beam and the bulk crystal. Therefore, the overall effect of the indentation mark on the test was small, in particular, smaller than the stress concentration effect at the corner between beam and bulk material.

The indentation mark was used to position the tool in a repeatable manner using the piezo-scanning feature of the indenter device in order to keep the moment arm identical in all experiments. The influence of these variations in the moment arm during loading caused about 5% maximum deviation in the measured stresses. The geometrically corrected moment arm is y_{corr}, as quantified in terms of the moment arm y, tool radius, R and indenter displacement d, i.e. $y_{corr} = y - R\tan(d/y)$.

A final macroscopic consideration might be to design longer beams for micromechanical bending tests as reported in earlier works [16,28]. From a continuum standpoint the use of longer beams could lead, in particular, to more homogeneous bending deformation. The drawback in manufacturing longer beams, however, lies in the risk of introducing more FIB-related surface damage that might entail undesired localization events. In addition, in a preceding paper we studied longer beams, which formed similar shear zones as observed in the present case owing to the crystallographic nature of the test [28].

4. Discussion

4.1. Stress–strain analysis and load drops: the mechanical Bauschinger effect

Extracting quantitative stress–strain and yield strength data from micrometer-scale elastic–plastic tests is challenging owing to the influence of potential variations in the external and internal boundary and initial value conditions [13,15,24,25,35–43]. Although such effects occur at all size scales, their relative influence increases as sample dimensions become smaller [33–35]. Specific challenges regarding the external boundary conditions arise from difficulties in controlling and monitoring the exactness in contact, loading, surface and shape change [24,35,41,45,47]. The control of the internal boundary conditions refers to the mapping of the microstructural state of a specimen before, during and after testing [15,25,35,37,46,47].

Regarding the Bauschinger data shown in Fig. 2, we analyzed a difference in yield stress between the first bending and first straightening steps of 73%. The second cycle was characterized by a yield stress drop of about 76% upon load reversal and the third cycle by about 83%. These huge changes in flow stress are larger than those typically reported for Bauschinger tests [1–6,13]. In view of the remarks made above it has to be underlined, however, that these absolute values represent upper bound estimates of the magnitude of the Bauschinger effect as they were taken from the back-extrapolation of stage I hardening to the elastic regime. Also, the experimental scatter in stress and moment arm determination must be considered when using these numbers.

Alternative, i.e. lower-bound, values of the yield stress drops upon load reversal were estimated by back-extrapolating the stage II hardening regimes of the elastic–plastic portion of the bending stress–strain curves. The onset of this regime is indicated by the blue arrows in Fig. 2. The coefficients of the linear fits are given in Table 1 in terms of p_1 and p_2, where d corresponds to the plastic strain. The reasoning behind the use of stage II hardening to derive a lower-bound measure of the Bauschinger effect (by back-extrapolation to the elastic regime) is the fact that it can be well approximated as a linear regime, while the early hardening stage in the first bending curve reveals stress drops, and hence cannot be easily fitted. Furthermore, owing to the influence of isotropic hardening upon further plastic cycling, the stage I/II transition can only be derived for the first loading curve (Fig. 2).

Using this second estimate yields smaller values for the yield stress drop upon load reversal compared to the upper bound evaluation of the Bauschinger effect where we used the back-extrapolation of the early hardening regime. It must be underlined though that the lower-bound estimate

is only a rough assumption as linear stage II hardening applies mainly to forward loading while it is unclear whether it also occurs during load reversal. The occurrence and magnitude of the athermal hardening contribution in Bauschinger tests may be profoundly different from conventional unidirectional tests. In addition, our results show that the forward hardening rates (bending step) that we extracted were significantly larger than the stage II hardening rates that are typically reported for bulk copper single crystals (210 MPa according to $G/200$ where G is the shear modulus with 42 GPa). The larger hardening values in our current sample are attributed to dislocation source limitation (source-related size effect). This effect is not relevant in macroscopic samples [28–30,37,41]. Evaluating these different aspects associated with the upper- and lower-bound estimates of the yield stresses and their decay upon load reversal assigns higher credibility to the upper bound estimates. The reason is that although the exact determination of the onset of plastic yielding for the upper-bound estimate can only be conducted at a precision of about 10 MPa, the corresponding stress–strain data are more reliable than those obtained from the linear back-extrapolation from stage II hardening owing to stress localization effects at the later deformation stages. In addition to the potential 10 MPa deviation, an additional error of about 5% must be conceded owing to the variations in the moment arm as explained above.

Irrespective of this error estimate the stress drops upon load reversal are large in the current case. The reason for this strong Bauschinger effect is the ability of the initially polarized dislocations to move backwards and carry plastic straining during reverse loading [7–9,48]. The fact that the stress drop is so pronounced is attributed to the phenomenon that the material deforms essentially under single slip conditions during forward bending (Figs. 3 and 4). This means that the parallel dislocations undergo little to no interaction with oblique slip systems. This means that the dislocations become polarized, as indicated by the KAM map in Fig. 2, but the degree of junction formation and entanglement remains very low. The first effect, namely the accumulation of polarized dislocation fields, creates strong long-range internal backstresses. These build up gradually during bending, resisting further forward loading, but they support plastic yielding when loaded in backward direction (straightening). The second effect, namely the weak entanglement, strongly reduces the yield strength when reversing the applied load. The thus enhanced availability of mobile dislocations without the necessity to extract them from tangles strongly reduces the requirement to activate new dislocation sources. This leads to a much softer reverse response and to a very smooth transition between the elastic and elastic–plastic regime in the reverse stress–strain curves when compared to observations made in earlier Bauschinger tests. For instance, in polycrystal deformation the accumulation of polarized dislocations occurs as well but single slip is not possible. Hence, a higher frequency of dislocation reactions, junctions, and tangles—due to multislip—leads to a lower availability of freely mobile dislocations and to a weaker difference between forward and reverse deformation. Besides the absolute levels of the stress changes upon load reversal observed in this work, Kiener et al. reported very similar findings on single-crystal Bauschinger tests [13]. In their work they found that the Bauschinger effect increases with increasing strain amplitude, increasing slip localization, and decreasing sample size [13].

The special role of single-crystal and single-slip effects in the current case also justifies to conduct a brief analysis of the steep load drops observed during forward bending (Figs. 2 and 5). The first bending curve reveals a number of pronounced force drops, indicating dislocation multiplication bursts that lead to strong shear localization (Figs. 3 and 4).

These sudden changes in the forces and stresses in the first bending curve (Figs. 2 and 5) resemble similar strain bursts that were observed during nanoindentation and several other micromechanical experiments [43,44]. The strong load drops that mark such burst events are due to the sudden availability of many dislocations that are formed after reaching a critical Frank–Read configuration. These dislocations, once created, do not require further load increase but easily sweep the glide plane, contributing a high local strain at a load level that is below the source activation force.

The first strain burst (Fig. 5, green arrow) is characterized by a force minimum that matches the force value measured upon reverse loading at the same strain (straightening step, Fig. 5, blue curve). As we assume that deformation upon load reversal is essentially carried by the reverse flow of free dislocations (without activating new sources), this observation supports the assumption that the minimum load values occurring during the bursts indeed represent the forces that are required for free dislocation motion (during forward loading) within the current microstructure. The local maximum loads at the onset of a strain burst are the source activation forces. For the first large strain burst (Fig. 5, green arrow) the difference in source activation stress and glide stress amounts to about 60 MPa (Fig. 2). The second very large load drop is characterized by a stress difference of about 120 MPa between source activation and glide (Fig. 2). At this point the stress drops from about 175 to 55 MPa. It is interesting to note in this context that for all three straightening curves, overall plastic yielding starts at about this stress level, i.e. between 45 and 55 MPa. This agreement is plausible as both the yield onset upon load reversal and the glide resistance at the load minimum of a strain burst event during forward bending characterize the motion of freely available glide dislocations where no source activation is required (until the next strain burst occurs). Analysis of the stress maximum values at the onset of the first strain bursts suggests a typical source length of about 600 Burgers vectors for the first bending test, 525 for the second one and 390 for the third one. Following earlier work on load drops in

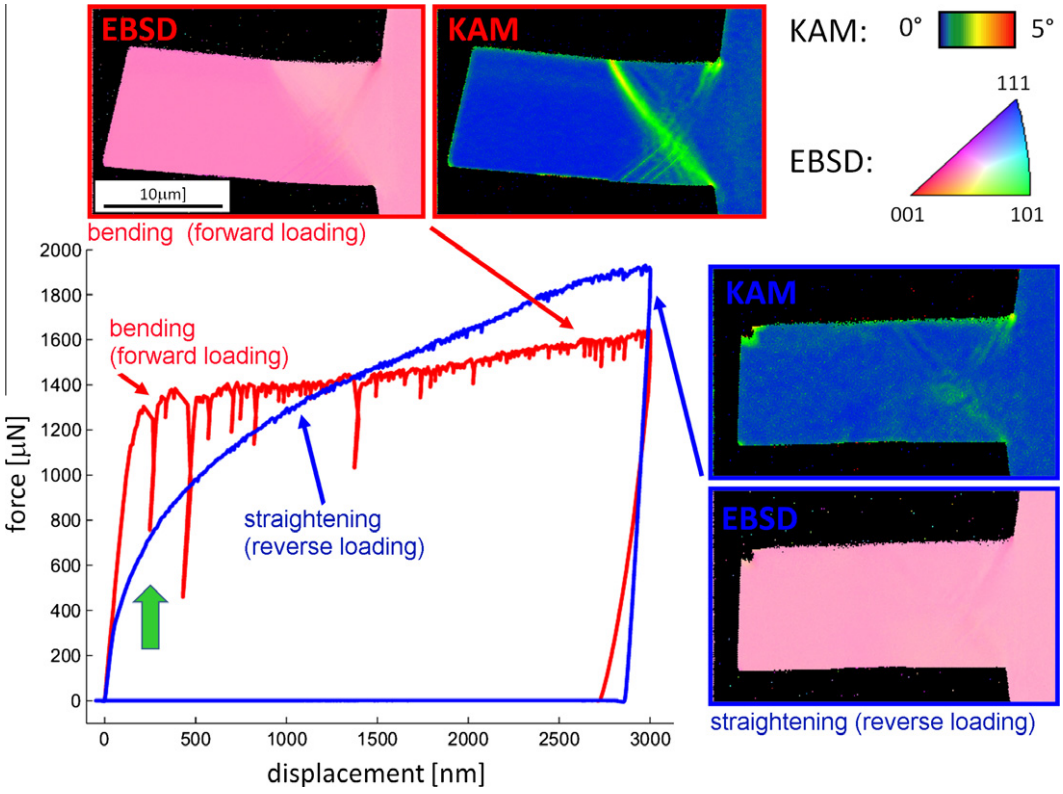

Fig. 5. Force–displacement curves of the first bending (red) and straightening cycle (blue) together with the complete microstructure maps (EBSD, KAM). The green arrow indicates a load drop where a strain burst occurs.

micromechanical tests it must be underlined however, that these strain bursts firstly, are statistical events, and secondly, are influenced by tensorial long-range internal stress fields that superimpose the machine load [43,44]. This means that an analysis of the source strength as indicated above can only provide a rough insight as both the influence of statistics and the internal stress levels are unknown in the current case.

The second and third deformation cycles are characterized by an overall higher stress level (Fig. 2) as the cross-hardening, which is relatively weak during the first cycle, accumulates during repeated loading.

4.2. Reversibility of misorientation gradient patterning upon load reversal: the microstructural Bauschinger effect

The Bauschinger effect does not only appear in the form of pronounced stress drops upon load reversal (Fig. 2), but also in terms of a remarkable restoration of the deformation-induced misorientation gradient patterning as documented in Figs. 3 and 5.

The KAM measure reveals the formation of weak and sharply localized misorientation gradient patterns along the primary slip system (Fig. 3, blue line) and a very pronounced and more broad misorientation gradient band along the minor slip system trace (Fig. 3, red line and ellipse). The formation of weak and sharply localized KAM traces (and hence GND arrays) along the major slip system is due to the small cross-hardening and negligible polarized dislocation storage along these slip traces. As discussed in the preceding section, forward bending proceeds via a sequence of strain bursts that produce polarized dislocations arrays on the same slip system, but only little strain hardening with oblique systems occurs. In contrast, the more broad and intense misorientation band that follows the minor slip system intersecting with the main slip system (Figs. 3 and 4) reveals a high accumulation of polarized debris of dislocations from the major system at its border. Fig. 4 indicates that the minor slip system itself contributes a relatively small amount of shear when compared to the main system which is active in a set of parallel microbands. The intense and broad misorientation gradient band that accompanies the slip trace of the minor system separates the tension from the compression zone. We assume that the GNDs assembled in this broad band are predominantly contributed by the slip activity in the leading slip system. In other words in both areas that are mainly sheared by the major slip system the dislocations pile up and polarize at the rim of the narrow shear zone created by the minor system (indicated by red ellipses in Fig. 3). Such misorientation gradient patterns have been observed previously in micro-scale bending experiments [28].

Upon load reversal, these pronounced misorientation gradient patterns are largely removed. This significant reduction in local lattice curvature (and hence in the amount of stored GNDs) after straightening the beam back

to its original shape suggests an easy activation of dislocation slip due to remobilization of the available GNDs that were formed and accumulated during the bending step. This is a situation where crystal plasticity becomes reversible through a large number of remobilized GNDs. It should be noted that this is a very unusual observation as plastic deformation, as a highly dissipative and irreversible process, shows here features of microstructure reversibility. This fact holds particularly for the misorientation gradient patterns that indicate accumulated GNDs (in terms of the KAM measure). The high degree of reversibility observed upon straightening is obviously due to the small influence of forest hardening for this particular orientation and loading situation.

In contrast to the removal of the GND content, as revealed by the KAM color map in Fig. 3, the grayscale image (Fig. 3, bottom) reveals irreversible distortions, i.e. lattice defects, that were not removed upon reverse loading. The grayscale image shows the EBSD pattern quality. It serves as a qualitative measure of lattice defects that affect the noise-to-signal ratio of the constructive interference patterns. We use it here as a rough indication of the dislocation content, although it has to be considered that it may also depend on surface contamination. Hence, we do not interpret these patterns quantitatively.

These two microstructural features allow the conclusion that the Bauschinger effect observed in the current case is characterized by the (incomplete) reversibility of the GND accumulation and the associated misorientation patterns and by the irreversibility of statistically stored dislocations. This observation is in very good agreement with the discussion of the stress–strain characteristics above. If we assume that the large Bauschinger effect is due to the fact that the polarized dislocations that were initially accumulated under (essentially) single forward slip can flow back at a low stress level upon load reversal, it is obvious that the associated misorientation patterns (which map the degree of polarization) will also decay. This exactly matches the current observation.

Based on this reasoning we suggest introducing the terminology of a "mechanical Bauschinger effect" and a "microstructural Bauschinger effect", where the former describes the drop in yield stress upon load reversal or load path changes, and the latter the degree and type of microstructure reversibility.

5. Summary and conclusions

We investigated the Bauschinger effect on a bent and straightened copper single crystal cantilever beam. We found a drop in yield strength upon reverse loading of up to 80%. The longitudinal beam surface was monitored using EBSD, KAM and slip-step analysis. The KAM data revealed pronounced misorientation patterning associated with shear localization and GND accumulation after bending. After reverse loading (straightening), the microstructure analysis showed that the GND arrays were removed (characterized in terms of the KAM analysis) but the statistically stored (non-polarized) dislocations remained (approximated qualitatively in terms of the EBSD pattern quality). Based on these observations we suggest a more precise terminology, namely a "mechanical Bauschinger effect" and a "microstructural Bauschinger effect", where the former term describes the drop in yield stress upon load reversal, and the latter the degree and type of microstructure reversibility upon load reversal.

References

[1] Hu XY, Chao W, Margolin H, Nourbakhsh S. Scripta Metall 1992;27:865.
[2] Yaguchi H, Margolin H. Scripta Metall 1983;17:1213.
[3] Stout MG, Rollett AD. Metall Trans 1990;21:3201.
[4] Hasegawa T, Yakou T, Kocks UF. Mater Sci Eng 1986;81:189.
[5] Kuhlmann-Wilsdorf D, Laird C. Mater Sci Eng 1977;27:137.
[6] Beyerlein IJ, Tome CN. Int J Plasticity 2007;23:640.
[7] Argon A. Strengthening mechanisms in plasticity. Oxford: Oxford University Press; 2007.
[8] Buckley SN, Entwistle KM. Acta Mater 1956;4:352.
[9] Hasegawa T, Yakou T, Karashima S. Mater Sci Eng 1975;20:267.
[10] Setoodeh AR, Attariani H. Mater Lett 2008;62:4266.
[11] Hou CT, Li ZH, Huang MS, Ouyang CJ. Acta Mater 2008;56:1435.
[12] Viatkina EM, Brekelmans WAM, Geers MGD. Int J Solids Struct 2007;44:6030.
[13] Kiener D, Motz C, Grosinger W, Weygand D, Pippan R. Scripta Mater 2010;63:500.
[14] Kim GS, Fivel MC, Lee HJ, Shin C, Han HN, Chang HJ, et al. Scripta Mater 2010;63:788.
[15] Motz C, Schoberl T, Pippan R. Acta Mater 2005;53:4269.
[16] Stölken JS, Evans AG. Acta Mater 1998;46:5109.
[17] Nye JF. Acta Metall 1953;1:153.
[18] Bilby BA, Gardner RT, Smith E. Acta Metall 1958;6:29.
[19] Kröner E. Int J Eng Sci 1963;1:261.
[20] Ashby MF. Philos Mag 1970;21:399.
[21] Kubin LP, Mortensen A. Scripta Mater 2003;48:119.
[22] El-Dasher BS, Adams BL, Rollett AD. Scripta Mater 2003;48:141.
[23] He JH, Luo JK, Le HR, Moore DF. Mater Sci Eng 2006;423:134.
[24] Dehm G, Motz C, Scheu C, Clemens H, Mayrhofer PH, Mitterer C. Adv Eng Mater 2006;8:1033.
[25] Motz C, Weygand D, Senger J, Gumbsch P. Acta Mater 2008;56:1942.
[26] Gong J, Wilkinson AJ. Acta Mater 2009;57:5693.
[27] Weber F, Schestakow I, Roters F, Raabe D. Adv Eng Mater 2008;8:37.
[28] Demir E, Roters F, Raabe D. Acta Mater 2010;58:1876.
[29] Greer JR, Oliver WC, Nix WD. Acta Mater 2005;53:1821.
[30] Shim S, Bei H, George EP, Pharr GM. Scripta Mater 2008;59:1095.
[31] Demir E, Raabe D, Zaafarani N, Zaefferer S. Acta Mater 2009;57:559.
[32] Calcagnotto M, Ponge D, Raabe D. Mater Sci Eng A 2010;527:2738.
[33] Raabe D, Ma D, Roters F. Acta Mater 2007;55:4567.
[34] Roters F, Eisenlohr P, Hantcherli L, Tjahjanto DD, Bieler TR, Raabe D. Acta Mater 2010;58:1152.
[35] Maaß R, Van Petegem S, Ma D, Zimmermann J, Grolimund D, Roters F, et al. Acta Mater 2009;57:5996.
[36] Budiman AS, Han SM, Greer JR, Tamura N, Patel JR, Nix WD. Acta Mater 2008;56:602.
[37] Dehm G. Prog Mater Sci 2009;54:664.
[38] Maass R, Van Petegem S, Van Swygenhoven H, Derlet PM, Volkert CA, Grolimund D. Phys Rev Lett 2007;99:145505.
[39] von Blanckenhagen B, Gumbsch P, Arzt E. Modell Simul Mater Sci Eng 2001;9:157.

[40] Kiener D, Grosinger W, Dehm G, Pippan R. Acta Mater 2008;56:580.
[41] Norfleet DM, Dimiduk DM, Polasik SJ, Uchic MD, Mills MJ. Acta Mater 2008;56:2988.
[42] Uchic MD, Shade PA, Dimiduk DM. Annu Rev Mater Res 2009;39:361.
[43] Shim S, Bei H, George EP, Pharr GM. Scripta Mater 2008;59:1095.
[44] Csikor FF, Motz C, Weygand D, Zaiser M, Zapperi S. Science 2007;318:251.
[45] Zaafarani N, Raabe D, Roters F, Zaefferer S. Acta Mater 2008;56:31.
[46] Zaafarani N, Raabe D, Singh RN, Roters F, Zaefferer S. Acta Mater 2006;54:1863.
[47] Raabe D, Ma D, Roters F. Acta Mater 2007;55:4567.
[48] Brown LM. Scripta Metall 1977;11:127.